

Supporting Information

A new family of cation-disordered Zn(Cu)-Si-P compounds as high-performance anodes for next-generation Li-ion batteries

Wenwu Li,^{a,b} Xinwei Li,^{*,c} Jun Liao,^a Bote Zhao,^b Lei Zhang,^b Le Huang,^a Guoping Liu,^a Zaiping Guo^d and Meilin Liu^{*,b}

- a. School of Materials and Energy, Guangdong University of Technology, Guangzhou 51006, China.
- b. School of Materials Science and Engineering, Georgia Institute of Technology, Atlanta, Georgia 30332, USA.
- c. Department of Mechanical and Energy Engineering, Southern University of Science and Technology, Shenzhen, 518071, China.
- d. Institute for Superconducting and Electronic Materials, School of Mechanical, Materials and Mechatronics Engineering, University of Wollongong, North Wollongong, NSW 2500, Australia.

Table S1. Crystallographic parameters and reliability factors for the cation-disordered ZnSiP₂ sample from XRD refinement.

Compound	ZnSiP ₂
Sp.Gr.	<i>F</i> -43 <i>m</i>
<i>a</i> , Å	5.34025
<i>V</i> , Å ³	152.3
2θ-interval, °	5-120
Number of reflections	13
Rwp, %	7.23
Rp, %	8.9
Rexp, %	2.67
χ^2	1.62
RB, %	1.77

Table S2. Fractional atomic coordinates and isotropic displacement parameters (Å²) of ZnSiP₂.

	x	y	z	<i>B</i> _{iso}	Occ.
P	0.25	0.25	0.25	1	1
Si	0	0	0	1	0.5
Zn	0	0	0	1	0.5

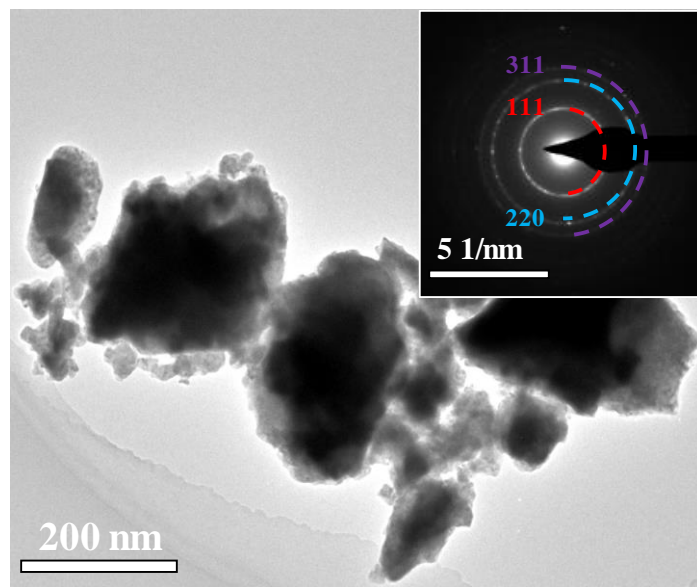


Figure S1. TEM image and the selected area electron diffraction (SAED) pattern of the cation-disordered ZnSiP₂ powder.

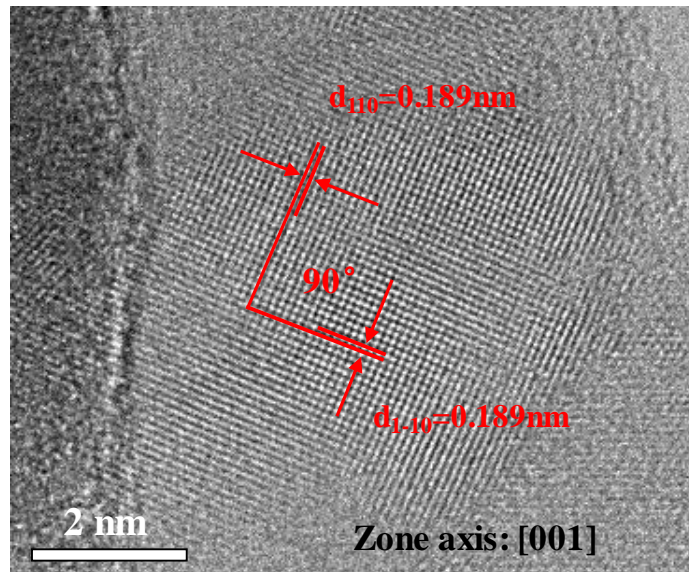


Figure S2. High-resolution TEM image of the cation-disordered ZnSiP_2 .

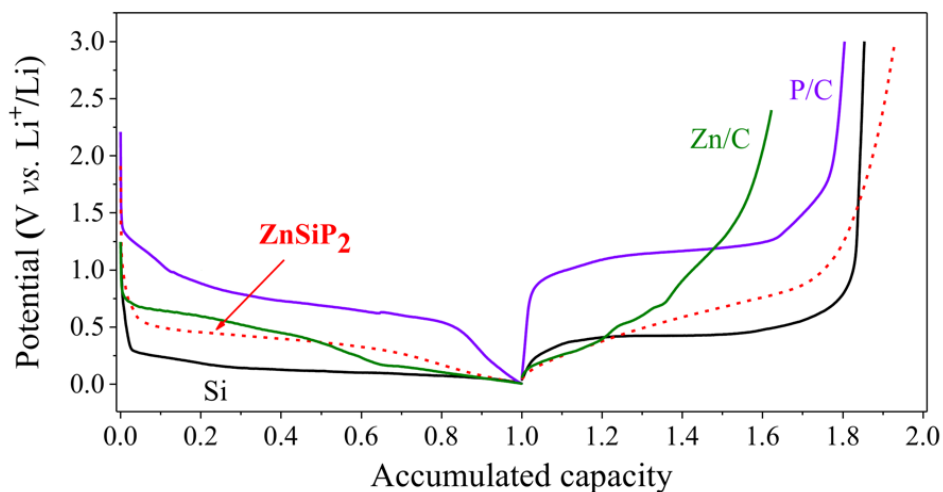


Figure S3. Discharge/charge profiles of the cation-disordered ZnSiP_2 , Zn/C , Si/C and P/C electrodes at a current density of 200 mA g^{-1} .

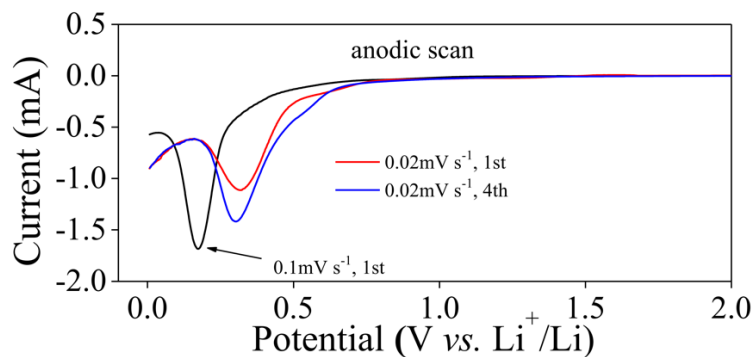


Figure S4. The initial anodic scan at different scan rates of the cation-disordered ZnSiP_2 anodes: black (Electrode 1), the initial anodic scan at a scan rate of 0.1 mV s^{-1} . Red (Electrode 2), the initial anodic scan at a scan rate of 0.02 mV s^{-1} ; blue (Electrode 2), the 4th anodic scan at a scan rate of 0.02 mV s^{-1} .

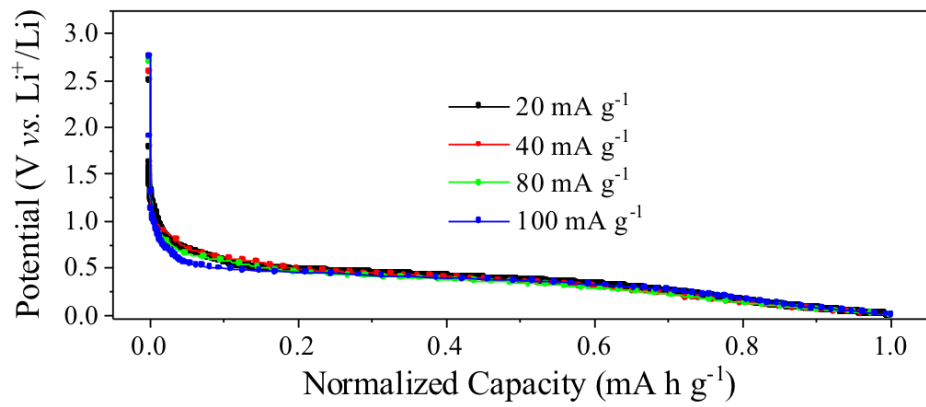


Figure S5. The initial discharge profiles of the ZnSiP₂ anodes cycled at ultralow current density of 20, 40, 80, and 100 mA g⁻¹.

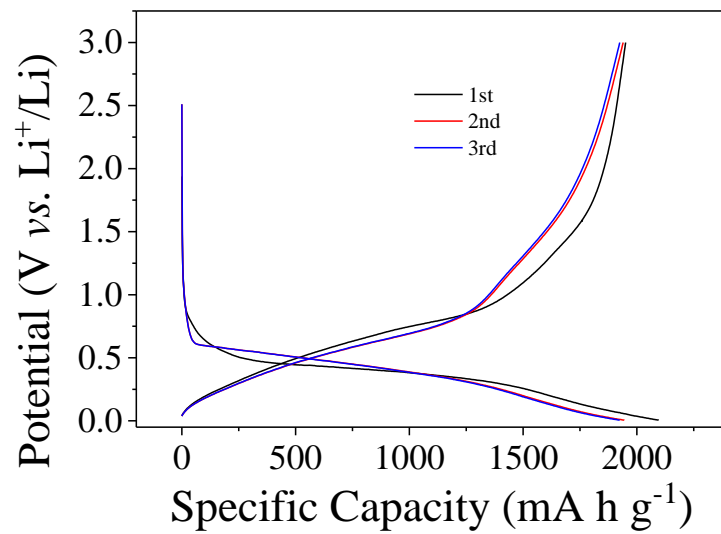


Figure S6. Initial three discharge/charge profiles of the cation-disordered ZnSiP₂ electrode at a current density of 200 mA g⁻¹

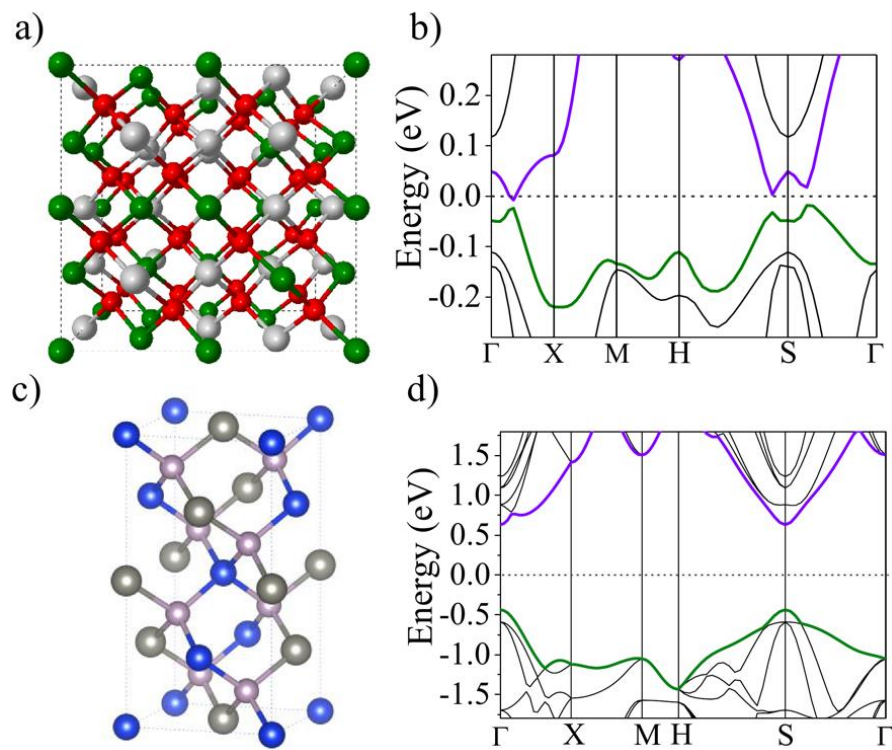


Figure S7. a) Schematic of the cation-disordered ZnSiP₂ crystal structure (red ball: P atom, gray white ball: Zn atom); b) the electronic structure based on the above model. c) the crystal structure model of the cation-ordered ZnSiP₂; d) the electronic structure of the cation-ordered ZnSiP₂.

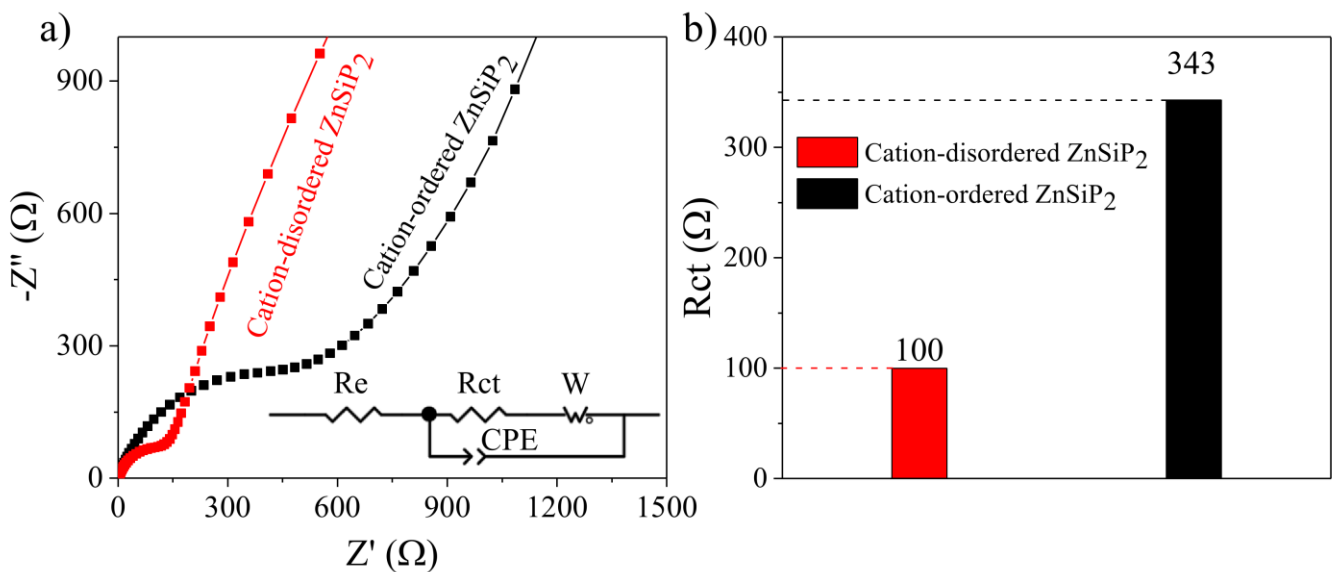


Figure S8. Electrochemical impedance spectroscopy study of a cation-disordered ZnSiP₂ electrode and a cation-ordered ZnSiP₂ electrode: a) impedance spectrum of a cell with a cation-disordered ZnSiP₂ electrode and that with a cation-ordered ZnSiP₂ electrode acquired under identical conditions, and b) charge transfer resistance (R_{ct}) determined from the impedance spectra shown in part a).

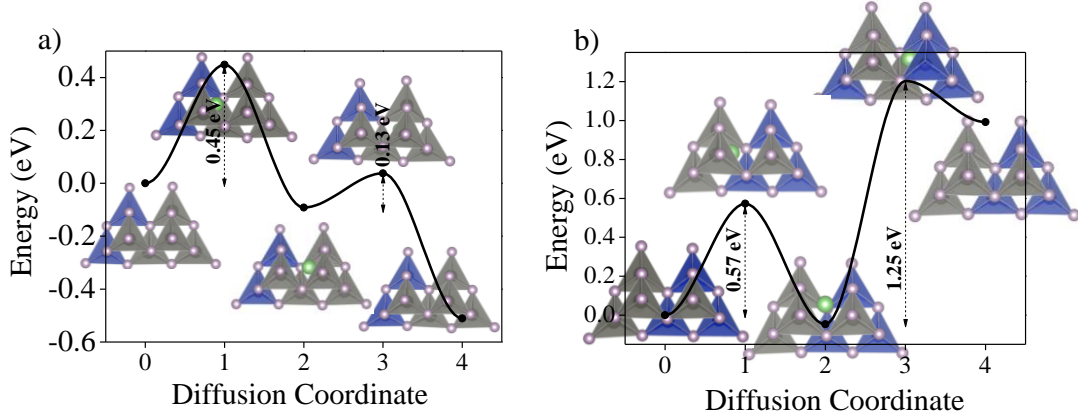


Figure S9. Li-ion diffusion barrier energy and its corresponding diffusion paths calculated based on the simulated model as shown in Figure S5a.

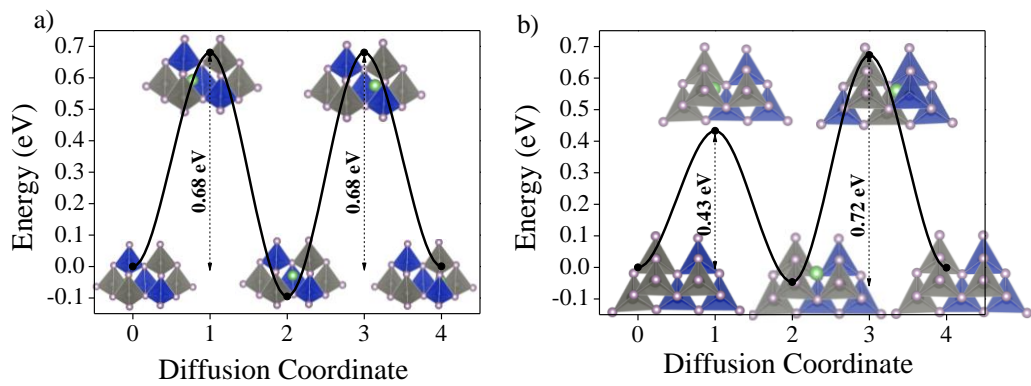


Figure S10. Li-ion diffusion barrier energy and its corresponding diffusion paths calculated based on the simulated model as shown in Figure S5c.

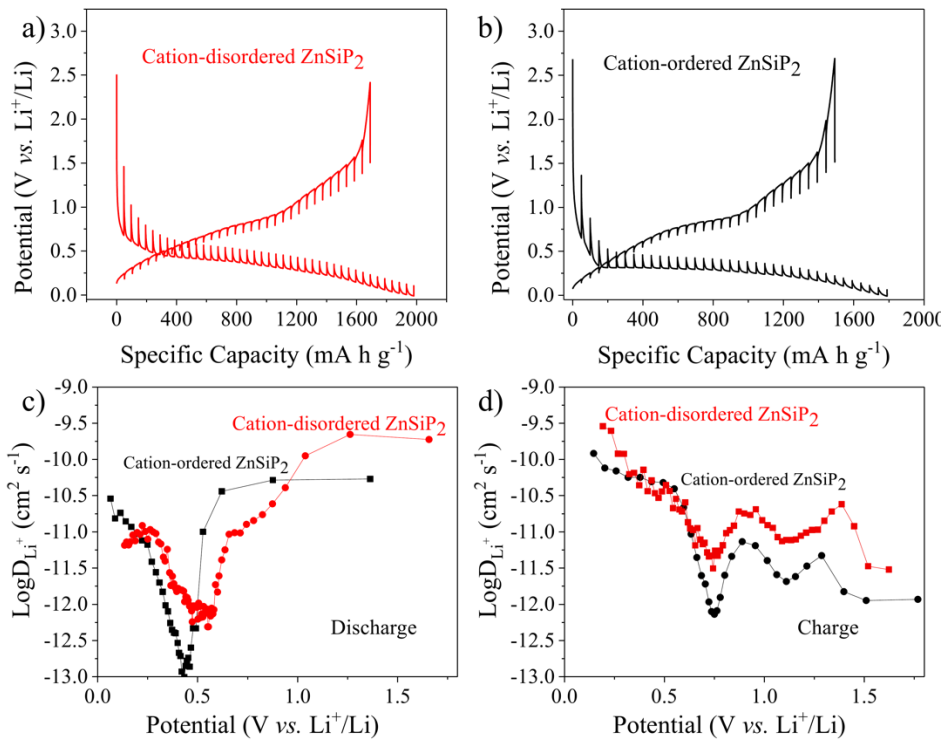


Figure S11. The cells were executed with a constant pulse for 30 min and then rest for 10 h: a) the initial discharge/charge profile of the cation-disordered ZnSiP₂ and b) the initial discharge/charge profile of the cation-ordered ZnSiP₂. Li-ion diffusion coefficients of the cation-disordered ZnSiP₂ and cation-ordered ZnSiP₂ anodes during discharge (c) and charge (d) processes.

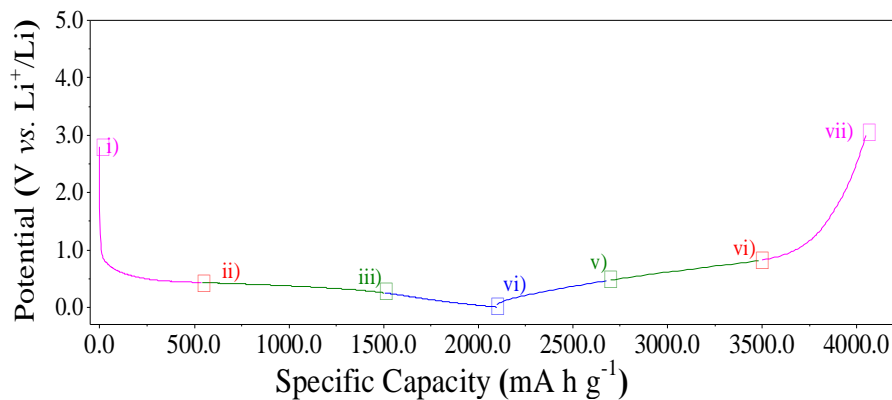


Figure S12. Discharge/charge profiles of the cation-disordered ZnSiP₂ used for ex-situ characterizations.

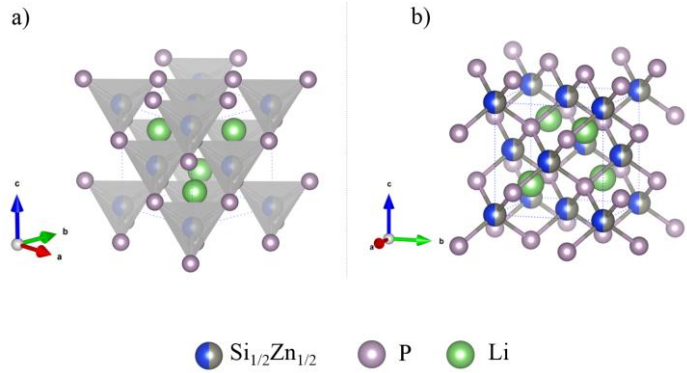


Figure S13. Schematic illustration of the voids suitable for Li-ion accommodation within the crystal structure of the cation-disordered $\text{Zn}_2\text{Si}_2\text{P}_4$ (one unit cell).

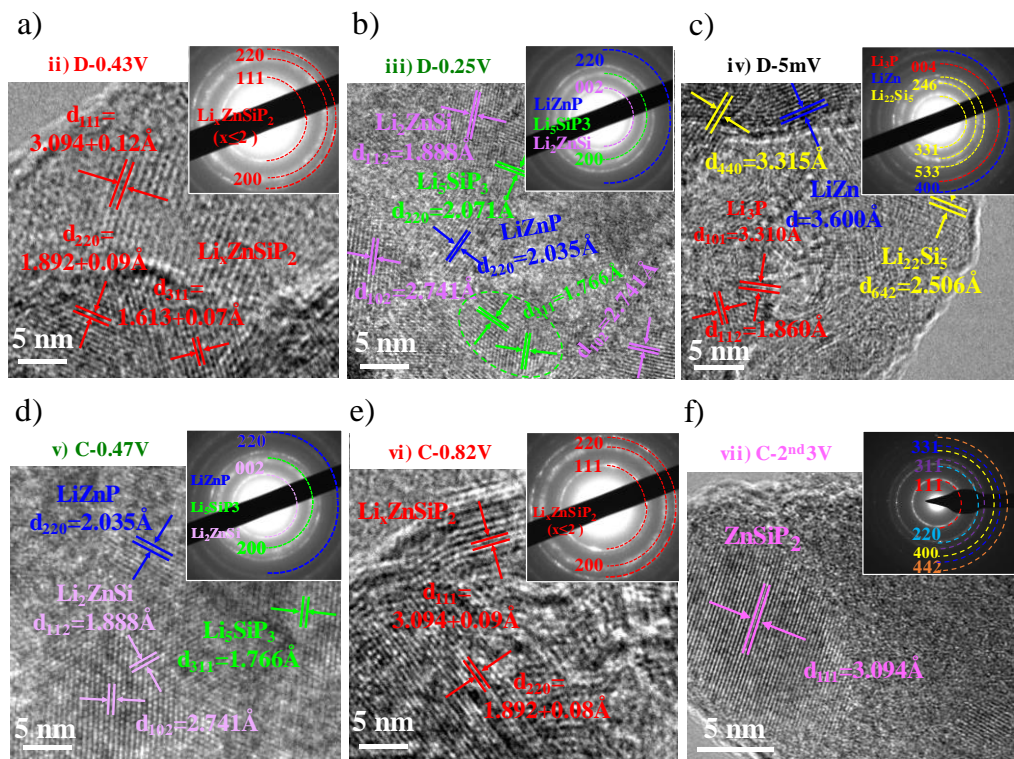


Figure S14. Ex-situ HRTEM and SAED patterns at the elected working potentials corresponding to Figure S9.

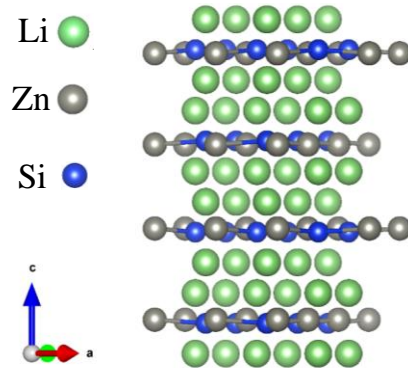


Figure S15. Schematic of the Li_2ZnSi crystal structure.

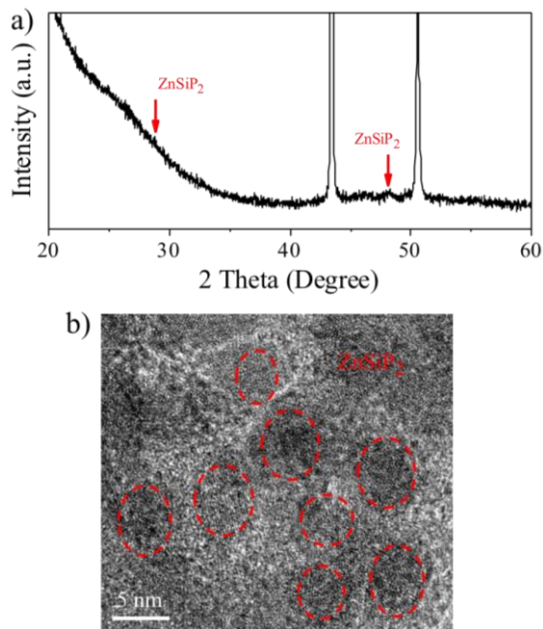


Figure S16. The ex-situ XRD (a) and HRTEM image (b) of the ZnSiP_2 electrode after 30 cycles.

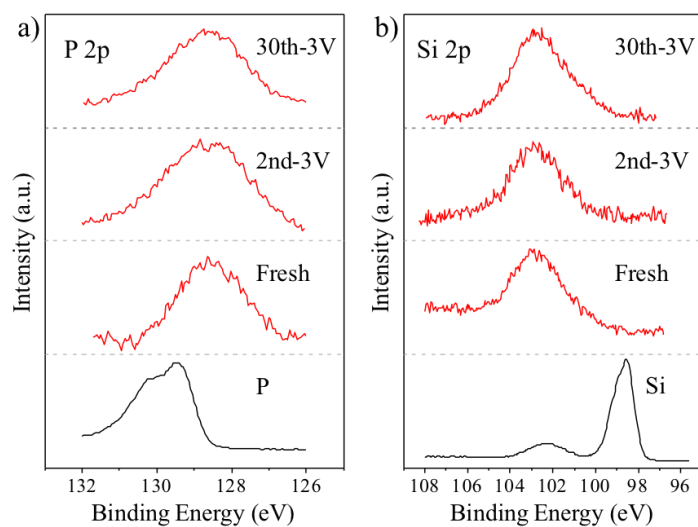


Figure S17. The ex-situ XPS of the ZnSiP_2 electrode after 30 cycles: a) high-resolution survey of P 2p; b) high-resolution survey of Si 2p.

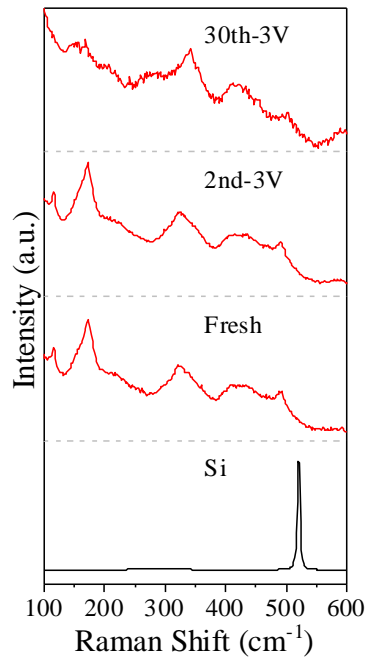


Figure S18. The ex-situ Raman of the ZnSiP_2 electrode after 30 cycles.

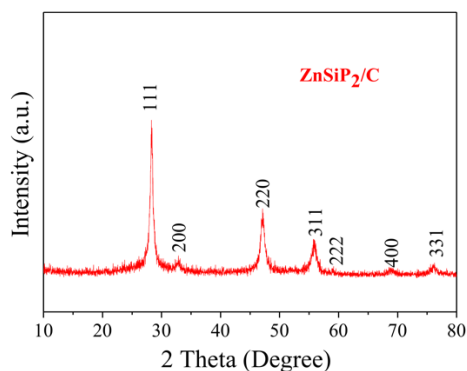


Figure S19. XRD pattern of the cation-disordered ZnSiP_2/C composite.

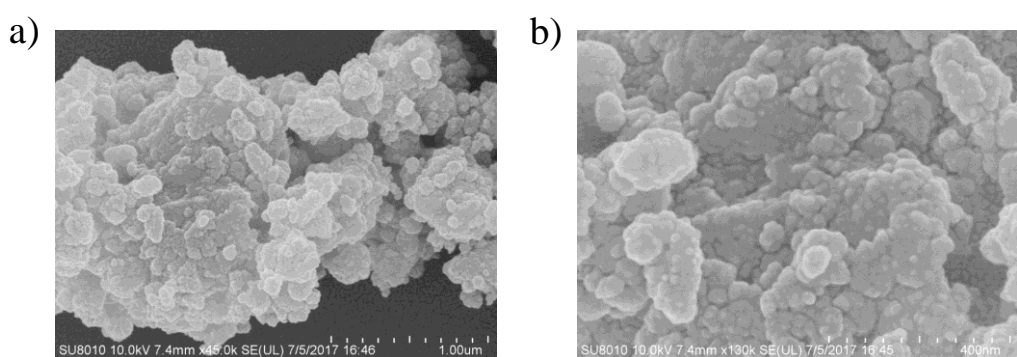


Figure S20. FSEM images of the cation-disordered ZnSiP_2 carbon composite: a) low-magnitude, b) high-magnitude.

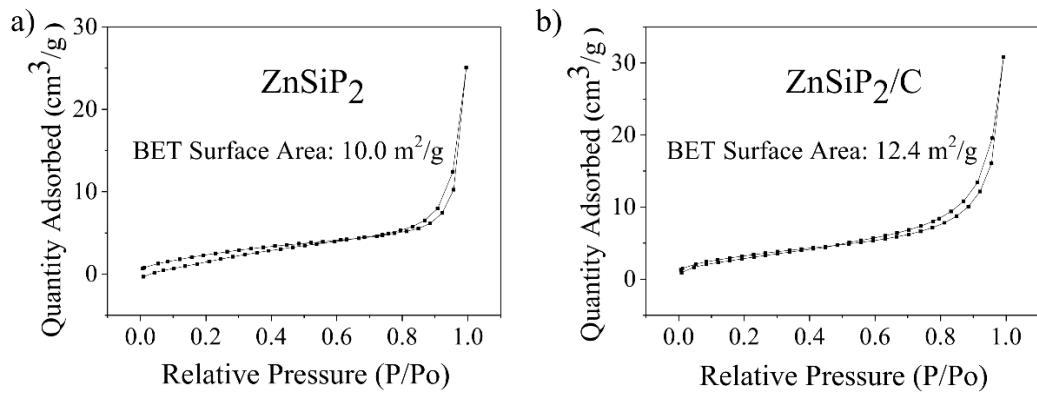


Figure S21. N₂ adsorption-desorption isotherms of a) the cation-disordered ZnSiP₂, and b) its carbon composite.

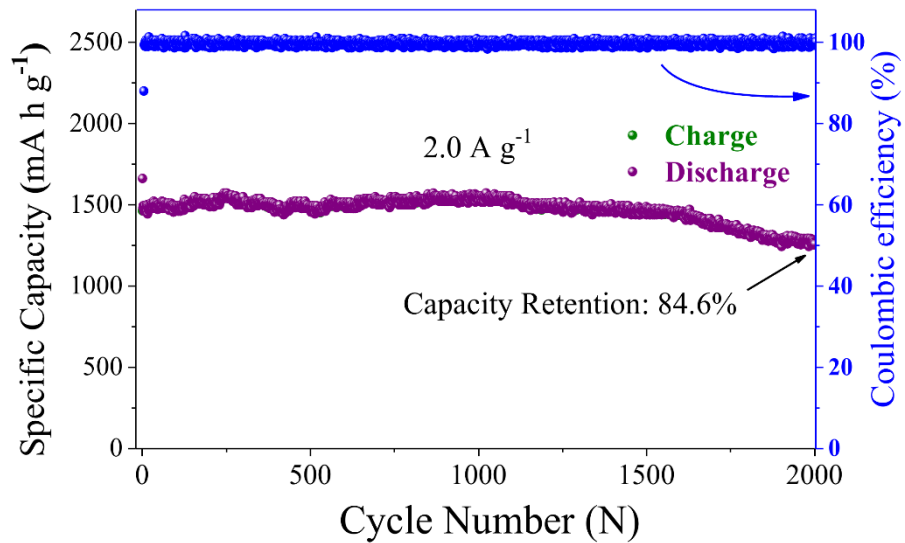


Figure S22. Cycle stability of the cation-disordered ZnSiP₂/C anode at the current density of 2000 mA g⁻¹.